SJSU SAN JOSÉ STATE UNIVERSITY

MTI MINETA TRANSPORTATION INSTITUTE

Time-To-Failure Prediction of Fine-Grained Soil Slopes Subject to Weather-Driven Deterioration

Amr M. Morsy, PhD, PE

California State University Transportation Consortium

CALIFORNIA STATE UNIVERSITY LONG BEACH

MINETA TRANSPORTATION INSTITUTE

Founded in 1991, the Mineta Transportation Institute (MTI), an organized research and training unit in partnership with the Lucas College and Graduate School of Business at San José State University (SJSU), increases mobility for all by improving the safety, efficiency, accessibility, and convenience of our nation's transportation system. Through research, education, workforce development, and technology transfer, we help create a connected world. MTI leads the Mineta Consortium for Transportation Mobility (MCTM) and the Mineta Consortium for Equitable, Efficient, and Sustainable Transportation (MCEEST) funded by the U.S. Department of Transportation, the California State University Transportation Consortium (CSUTC) funded by the State of California through Senate Bill 1 and the Climate Change and Extreme Events Training and Research (CCEETR) Program funded by the Federal Railroad Administration. MTI focuses on three primary responsibilities:

Research

MTI conducts multi-disciplinary research focused on surface transportation that contributes to effective decision making. Research areas include: active transportation; planning and policy; security and counterterrorism; sustainable transportation and land use; transit and passenger rail; transportation engineering; transportation finance; transportation technology; and workforce and labor. MTI research publications undergo expert peer review to ensure the quality of the research.

Education and Workforce Development

To ensure the efficient movement of people and products, we must prepare a new cohort of transportation professionals who are ready to lead a more diverse, inclusive, and equitable transportation industry. To help achieve this, MTI sponsors a suite of workforce development and education opportunities. The Institute supports educational programs offered by the Lucas Graduate School of Business: a Master of Science in Transportation Management, plus graduate certificates that include High-Speed and Intercity Rail Management and Transportation Security Management. These flexible programs offer live online classes so that working transportation professionals can pursue an advanced degree regardless of their location.

Information and Technology Transfer

MTI utilizes a diverse array of dissemination methods and media to ensure research results reach those responsible for managing change. These methods include publication, seminars, workshops, websites, social media, webinars, and other technology transfer mechanisms. Additionally, MTI promotes the availability of completed research to professional organizations and works to integrate the research findings into the graduate education program. MTI's extensive collection of transportation-related publications is integrated into San José State University's world-class Martin Luther King, Jr. Library.

Time-To-Failure Prediction of Fine-Grained Soil Slopes Subject to Weather-Driven Deterioration

Amr M. Morsy, PhD, PE

August 2024

TECHNICAL REPORT
DOCUMENTATION PAGE

1. Report No. 24-20	2. Government Accession No.	3. Recipient's Catalog No.

4. Title and Subtitle		5. Report Date
Time-To-Failure Prediction of Fine-Grained Soil Slopes Subject to Weather-Driven Deterioration		August 2024
		6. Performing Organization Code

7. Authors	8. Performing Organization Report
Amr M. Morsy, PhD, PE	CA-MTI-2326

9. Performing Organization Name and Address	10. Work Unit No.
Mineta Transportation Institute College of Business San José State University San José, CA 95192-0219	
	11. Contract or Grant No. ZSB12017-SJAUX

12. Sponsoring Agency Name and Address	13. Type of Report and Period Covered
State of California SB1 2017/2018 Trustees of the California State University Sponsored Programs Administration 401 Golden Shore, 5th Floor Long Beach, CA 90802	
	14. Sponsoring Agency Code

15. Supplemental Notes
10.31979/mti.2024.2326

16. Abstract
Embankments have been widely used in the construction of transportation and flood defense infrastructure. Embankments constructed from clays experience a suite of weather-driven deterioration processes that lead to a progressive loss of hydromechanical performance, causing potentially severe and costly consequences. This study aimed to predict the time to failure of aging, deteriorating clay embankments supporting transportation infrastructure. A multi-phase numerical modeling approach was developed to replicate the long-term, weather-driven, hydromechanical behavior of clay embankments. This model simulated the behavior of a number of well-documented embankment failure case studies that had sufficient data to derive the necessary soil properties and climate records. Numerical models were developed for a total of 34 case studies, and numerical simulations were performed to predict their time to failure. Predictions compared well with the actual times to failure reported for the simulated case studies. Overall, the numerical modeling approach proved efficient in developing deterioration models that could improve infrastructure asset management. Practical recommendations are provided based on the findings of this study.

17. Key Words	18. Distribution Statement
Embankments, Slope failure, Earthwork, Weathering, Deterioration by environmental action	No restrictions. This document is available to the public through The National Technical Information Service, Springfield, VA 22161.

19. Security Classif. (of this report)	20. Security Classif. (of this page)	21. No. of Pages	22. Price
Unclassified	Unclassified	45	

Form DOT F 1700.7 (8-72)

ACKNOWLEDGMENTS

CONTENTS

LIST OF FIGURES

LIST OF TABLES

Executive Summary

Embankments are crucial components of transportation and flood defense infrastructure, yet those constructed from clays are prone to weather-driven deterioration processes, resulting in gradual loss of hydromechanical performance and potentially severe failures. This report documents a study aimed to predict the time to failure of aging clay embankments supporting transportation infrastructure. This report is intended for infrastructure stakeholders and practicing engineers, particularly those located in California. In this study, a multi-phase numerical modeling approach was used to simulate the long-term, weather-driven, hydromechanical behavior of clay embankments of well-documented failure case studies. Numerical models were developed for 34 case studies, and simulations predicted the time to failure due to progressive deterioration. This modeling approach proved efficient in producing data necessary for improving infrastructure asset management. Based on the observations from the numerical results, it is recommended that a Factor of Safety (FoS) target against weather-driven shallow slides is introduced in evaluating the stability of existing embankment slopes and new embankment slopes.[1] Considering the typical recommended minimum FoS values by Caltrans, an FoS of 1.1 to 1.2 may be reasonable for existing embankments, given the temporary nature of conditions causing shallow slides. For new designs, an FoS of 1.3 may be recommended.

---

[1] Factor of Safety (FoS) is an engineering measure of the stability of a slope typically used in civil engineering practice. An FoS of 1.0 corresponds to a limit equilibrium condition below which failure happens.

1. Introduction and Background

Slopes with significant lengths have been constructed since the 1800s to support infrastructure such as railways, highways, and flood embankments. Unexpected failures of deteriorating, aged infrastructure can have severe societal and economic consequences and can, in the worst cases, lead to fatalities (e.g., Baral and Shahandashti 2022). Slope failures in earth infrastructure occur frequently, and globally, cause approximately $4 billion in property damage and nearly 1000 human casualties every year (Zhang et al., 2019). Financial and carbon costs associated with repair are significant. The emergency repairs can cost up to ten times more than regular maintenance, with average costs for emergency work being approximately three times more expensive per running unit length than planned renewals (Glendinning et al., 2009; ORR, 2021). In the 1990s, the annual repair costs of US highways due to landslides was estimated to be at least $106 million (Walkinshaw, 1992). The annual losses average approximately $200 million from slope/ground failure and flooding in California for years in which rainfall exceeds 140% of normal (Slosson and Larson 1995). In the 2018 fiscal year, the repair costs of slopes along the Texas highway corridors were reported to be $28.5 million (Shahandashti et al., 2019). A recent example from California is the collapse of the Pacific Coast Highway (PCH) near Big Sur in 2021 following a rainstorm; this failure created months of financial and societal disruptions. According to a recent report published by the National Cooperative Highway Research Program (NCHRP) of the Transportation Research Boards, "the management of bridge and pavement assets has for many years garnered significant attention by state transportation agencies while the management of geotechnical assets—such as walls, slopes, embankments, and subgrades—has been elusive" (NASEM, 2019).

1.1 Overview of the Problem

The performance of infrastructure assets supported by soil slopes is affected by time-dependent deterioration processes of soils. It is evident that weather-driven deterioration mechanisms contribute significantly to the overall deterioration of earth infrastructure assets, which has resulted in a body of research on the deterioration of slopes, where weather cycles can lead to progressive failure (e.g., Templeton et al. 1984; Vaughan et al. 2004; Nyambayo et al., 2004; Rouainia et al., 2009; Nyambayo and Potts, 2010; Kovacevic et al., 2013; Postill et al., 2021; Morsy et al., 2023a). Weather-related deterioration mechanisms cause adverse changes in hydromechanical behavior that include strength reduction (Skempton, 1964), desiccation cracking (Anderson et al., 1982; Cheng et al., 2020; Morsy et al., 2024), downslope ratcheting (Take and Bolton, 2011; Lees et al., 2013), softening of clay lumps during wet seasons (Skempton, 1996), and reorientation of clay particles (Kayyal and Wright, 1991). Tang et al. (2018) summarized the key deterioration mechanisms as surface and internal erosion, surface cracking, freeze-thaw action, wetting, and shrink-swell behavior. Stirling et al. (2021) demonstrated that deterioration results from exceedance of the previous maximum stress experienced by the material and that deterioration mechanisms can be grouped into four interdependent categories: (1) irrecoverable micro-structure deformation, which alters clay fabric through soil aggregation and desiccation cracking; (2) changes in soil-water retentivity and hydraulic permeability; (3) loss in strength; and (4) macro-

scale deformation, which results in strain softening. Further, deterioration processes may involve different types of mechanisms that may have different onsets and progress at different rates. Collectively, these mechanisms contribute differently to the overall deterioration rate of an infrastructure asset at a given time during the service life of the asset. A similar concept was adopted for structural assets including steel and concrete structures (Biondini and Frangopol, 2016). It is inevitable that climate change will alter the weather patterns, and hence the weather-driven deterioration rates of infrastructure. Accordingly, the California Department of Transportation (Caltrans) has plans to analyze the effects of climate change on the state's transportation infrastructure. These plans are intended to "translate the state of climate science into useful information for action" across the state and is presented in California's Fourth Climate Change Assessment (Bedsworth et al., 2018).

While significant advances have been made in the understanding of element- and asset-scale deterioration of earth infrastructure, further investigations and rigorous analyses of slope failures are needed (e.g., Briggs et al., 2017). Current practice requires enhanced capabilities to forecast future performance and the remaining service life of aging infrastructure. These capabilities would take the form of robust and reliable modeling approaches that can account for weather-driven deterioration under a range of climate projections. According to the California Transportation Asset Management Plan (TAMP, 2022), opportunities identified for future improvements in transportation asset management include "enhancing asset modeling capabilities." Ultimately, such capabilities will enable proper planning for the allocation of maintenance resources to minimize disruption and costs. Asset-scale numerical models that incorporate weather-driven deterioration mechanisms, which have been observed at the element-scale in the laboratory (e.g., Stirling et al., 2021), can enable the forecasting of the remaining service life of earth infrastructure assets.

1.2 Research Objectives

This study aims to provide enhanced asset modeling capabilities for soil slopes used in supporting transportation infrastructure assets by providing a practical tool that can be used to forecast the time to failure for the slopes of clay embankments. Specifically, an asset-scale numerical model was developed to incorporate weather-driven deterioration mechanisms. This numerical model was based on a robust numerical modeling approach that simulates the construction and long-term, weather-driven hydromechanical behavior of clay slopes. The numerical model was validated previously by Morsy et al. (2023a, b), using laboratory tests and nine years of measurements from a full-scale embankment. While the numerical model is able to capture the weather-driven deterioration mechanisms in soil slopes, it has not yet been validated for its ability to predict the time to failure of slopes, which is necessary to be able use the model confidently in failure prediction. The objective of this study is to use the developed and validated numerical modeling approach to enable forecasting of the time to failure of fine-grained soil slopes prone to weather-driven deterioration. Specifically, the numerical model was used to simulate several, well-documented case histories of slope failures to assess the ability of the numerical model to predict the age of these slopes at failure.

This study consists of (1) a review and evaluation of the existing slope deterioration models that are used by infrastructure stakeholders in the US, particularly those located in the state of California; (2) development of a database of well-documented slope failure case studies; (3) development of computer models for the slope failure case studies; and (4) practical recommendations.

1.3 Report Organization

This report consists of six sections:

- Section 1. Introduction and Background: This section presents the overview of the problem and research questions, research aim and objectives, and report organization.

- Section 2. Embankment Attributes and Shallow Failures: This section discusses embankment surficial failures in California, embankment design in California, and summarizes the engineering properties of compacted fills.

- Section 3. Case Studies of Embankment Failures: This section compiles the attributes of 34 embankment failure case studies.

- Section 4. Computer Models: This section documents the development of numerical models used to simulate the long-term behavior of the 34 compiled case studies from construction to failure.

- Section 5. Failure Prediction: This section presents and discusses the results of the numerical simulations of the 34 case studies.

- Section 6. Summary and Recommendations: This section summarizes the study documented in this report and provides practical recommendations based on its findings.

This report was written for infrastructure stakeholders and practicing engineers with the exception of Sections 3, 4, and 5 which were written primarily for practicing engineers.

2. Embankment Attributes and Shallow Failures

Slopes are used to support a wide range of infrastructure in the US and globally, including embankments for highways, railways, dams, and levees. Since slopes serve infrastructure, whose safety is deemed a matter of public safety and national security, state DOTs have developed extensive experience on how to monitor and inspect their infrastructure assets on a frequent basis.

2.1 Embankment Surficial Failures in California

A recent survey was administered by Beckstrand and Bunn (2024) as part of an NCHRP synthesis on surficial (i.e., shallow) embankment failures. Survey responses by California personnel documented by Beckstrand and Bunn (2024) are summarized next:

- The state regularly experiences surficial embankment failures. Approximately, 80% of embankment failures in California embankments are considered surficial (less than 10 ft deep) and 20% are considered deep-seated (larger than 10 ft deep).

- The state is responsible for approximately 15,092 road miles, 40% of which are estimated to be susceptible to surficial failures. No inventories of embankment attributes (height, length, side-slope angles, material, year of construction) or embankment failures (occurrence, measurements, repair method) are maintained.

- Approximately, 60% of the embankments have not required maintenance nor suffered surficial instabilities since original construction, 10% have required periodic maintenance due to surficial instabilities, 10% have suffered surficial instabilities but have not received remedial treatment, 18% have received remedial treatment for surficial instabilities and are functioning as originally designed after treatment, and 2% have received remedial treatment for surficial instabilities but are not functioning as originally designed after treatment.

- Causes of surficial failures in California include, in order of importance, (1) poorly controlled surface drainage, (2) poorly armored, maintained, or designed culvert outlets, (3) undermining toe of slope due to stream or river scour, (4) wildfire-induced changes to embankment surface drainage characteristics, (5) poor subsurface drainage, and (6) poor compaction.

- Surficial embankment failures commonly occur following severe weather events or a pattern of events (Beckstrand and Bunn, 2024). California reported that there may be a relationship between failures that occurred in the state and (1) continuous rainfall (frequent rain events over a several-week period), (2) heavy rainfall, and (3) snowmelt/rain on snow. The approximate time to surficial failure due to embankment fill or drainage deterioration in California is 20 to 40 years, assuming the original design and construction was appropriate for the materials used and the site conditions.

- California respondents confirmed the existence of some design standards related to prevention or repair of surficial embankment failures. New embankment design within California is addressed by design manuals, standard drawings, specifications, and standard preventative measures. No recommended target design factor of safety is set for the surficial stability during embankment design. However, a factor of safety of 1.3 is required during surficial embankment repairs. No consideration is given to unit weight surcharge caused by top-down saturation during heavy precipitation. (The wetting front would contribute additional mass rather than pore water pressure at the shear zone.) Limit equilibrium is used for analysis of surficial stability. Software applications include GeoStudio Slope/W and Rocscience Slide. A target side slope would be the desired slope if no right-of-way or foundation constraints were to influence embankment design. A commonly used target side slope is 4H:1V, which the FHWA generally considers a recoverable slope (Beckstrand and Bunn 2024). It is believed that 4H:1V is the recommended target sides slope for embankments from the California Landscape Architecture unit, and a maximum recommended sides slope is 1.5H:1V from the California Geotechnical unit.

- Proactive measures are used in California to prevent or reduce the likelihood of surficial instability when constructing new embankments. These measures include, in the order of common usage, hydroseed, draped degradable matting, riprap or rock blankets/plating, cellular confinement systems (e.g., geocells), and anchored turf reinforcement mat. Of these measures, the most cost-effective systems with the highest success rates are the draped degradable matting, riprap, or rock blankets/plating, and cellular confinement systems. For repair of failed embankments, riprap or rock blankets/plating, rock inlays, and buttresses were reported to have provided cost-effective repair/treatment function with a high success rate.

- Approximately, 20% of surficial slope failure repairs involved engineering design, 35% of which are provided by agency in-house professionals, 5% are provided by consultants, and 60% are preventative and repair measures performed as maintenance activities without engineering design. When surficial slope failures occur, 60% are repaired by agency maintenance crews and 40% by construction contractors.

2.2 Embankment Design in California

Geotechnical considerations for embankment design and construction involve assessments of the stability and settlement of the foundation soils, understanding how these factors affect the construction staging and time requirements, and evaluating potential impacts on nearby structures such as buildings, bridge foundations, and utilities. It is essential for the investigation to include the embankment area and at least two to three times the width of the embankment on either side.

As per Caltrans Highway Design Manual (2020), the relative compaction of embankment fills must be at least 95%. Select materials, local and/or imported borrow, may be recommended to assure that the compaction requirements are met and that shrink/swell problems are avoided.

Embankments should be constructed in layers, where the loose thickness of each layer must not exceed eight inches. As per Caltrans Geotechnical Manual (2014), Landscape Architecture may request, with careful consideration, reduced compaction requirements from 90-95% relative compaction to 85-88% relative compaction to promote the growth of vegetation on embankment slopes.

As per Caltrans Geotechnical Manual (2014), earth embankments ten feet or less in height with 2H:1V or flatter side slopes may be designed based on past precedents and engineering judgment, provided there are no known problem soil conditions such as organic soils, soft/ loose soils, potentially unstable soils, such as Bay Mud or peat, or liquefiable sands. Embankments over ten feet in height, embankments with side slope inclinations steeper than 2H:1V, or embankments on soft soils, in unstable areas/soils, or those comprised of lightweight fill require more in-depth stability analyses. As per Caltrans Highway Design Manual (2020), embankment end slopes at open-end structures should be no steeper than 1½H:1V for all highways. As per the Caltrans Geotechnical Manual (2014), typical recommended FoS values are as follows:

- Highway embankments that neither support nor potentially impact structures should have a minimum FoS of 1.25. When repairing an embankment slide or slip-out, and a factor of safety for the embankment can be reliably calculated, a minimum FoS of 1.15 may be used.

- Highway embankments that support or potentially impact structures should have a minimum FoS of 1.30.

- Bridge approach embankments and embankments supporting important structures should have a minimum FoS of 1.50.

- Temporary embankments during construction can have a minimum FoS lower than they would over the longer term, typically about 1.10 to 1.20.

2.3 Engineering Properties of Compacted Soils

In the FHWA-HIN-21-002 report, Samtani and Nowatzki (2021) synthesized typical values for the engineering properties of compacted soils for 14 different USCS designations. The values of the engineering properties refer to soils compacted to maximum dry density by the standard Proctor test. The synthesized data were based on more than 1,500 soil tests performed by the Bureau of Reclamation, as reported in USBR (1960). The majority of the soils were from 17 western states in the United States. Samtani and Nowatzki (2021) emphasized that the shear strength parameters in Table 1 must not be used for design and that project-specific testing must be performed to develop the design shear strength parameters. The values of the engineering properties reported in Table 1, however, are valuable in developing statistical designs when considering parametric evaluations.

Table 1. Average Engineering Properties of Compacted Inorganic Soil
(Samtani and Nowatzki 2021 after USBR 1960 and FHWA 2006)

Soil No.	USCS	Standard Proctor Maximum Dry Density (MDD or γ_{dmax}), pcf (kN/m³)	Standard Proctor Optimum Moisture Content, w_{opt} (%)	As Compacted Effective Cohesion, c_0 psi (kPa)	Compacted-Saturated Effective Cohesion, c_{sat} psi (kPa)	Friction Angle, ϕ (deg)	Void Ratio, e [Permeability, k (ft/yr)]
1	GW	>119 (>18.7)	<13.3	*	*	>38	* [27,000 ± 13,000]
2	GP	>110 (>17.3)	<12.4	*	*	>37	* [64,000 ± 34,000]
3	GM	>114 (>17.9)	<14.5	*	*	>34	* [> 0.3]
4	GC	>115 (>18.1)	<14.7	*	*	>31	* [> 0.3]
5	SW	119 ± 5 (18.7 ± 0.8)	13.3 ± 2.5	5.7 ± 0.6 (39 ± 4)	*	38 ± 1	0.37 ± * [*]
6	SP	110 ± 2 (17.3 ± 0.3)	12.4 ± 1.0	3.3 ± 0.9 (23 ± 6)	*	37 ± 1	0.50 ± 0.03 [>15.0]
7	SM	114 ± 1 (17.9 ± 0.2)	14.5 ± 0.4	7.4 ± 0.9 (51 ± 6)	2.9 ± 1.0 (20 ± 7)	34 ± 1	0.48 ± 0.02 [7.5 ± 4.8]
8	SM-SC	119 ± 1 (18.7 ± 0.2)	12.8 ± 0.5	7.3 ± 3.1 (50 ± 21)	2.1 ± 0.8 (14 ± 6)	33 ± 4	0.41 ± 0.02 [0.8 ± 0.6]
9	SC	115 ± 1 (18.1 ± 0.2)	14.7 ± 0.4	10.9 ± 2.2 (75 ± 15)	1.6 ± 0.9 (11 ± 6)	31 ± 4	0.48 ± 0.01 [0.3 ± 0.2]
10	ML	103 ± 1 (16.2 ± 0.2)	19.2 ± 0.7	9.7 ± 1.5 (67 ± 10)	1.3 ± * (9 ± *)	32 ± 2	0.63 ± 0.02 [0.59 ± 0.23]
11	ML-CL	109 ± 2 (17.1 ± 0.3)	16.8 ± 0.7	9.2 ± 2.4 (63 ± 17)	3.2 ± * (22 ± *)	32 ± 3	0.54 ± 0.03 [0.13 ± 0.07]
12	CL	108 ± 1 (17.0 ± 0.2)	17.3 ± 0.3	12.6 ± 1.5 (87 ± 10)	1.9 ± 0.3 (13 ± 2)	28 ± 2	0.56 ± 0.01 [0.08 ± 0.03]
13	MH	82 ± 4 (12.9 ± 0.6)	36.3 ± 3.2	10.5 ± 4.3 (72 ± 30)	2.9 ± 1.3 (20 ± 9)	25 ± 3	1.15 ± 0.12 [0.16 ± 0.10]
14	CH	94 ± 2 (14.8 ± 0.3)	25.5 ± 1.2	14.9 ± 4.9 (103 ± 34)	1.6 ± 0.86 (11 ± 6)	19 ± 5	0.80 ± 0.04 [0.05 ± 0.05]

Notes:
(a) The entry ± indicates 90 percent confidence limits of the average value; * denotes insufficient data.
(b) For permeability, 1 ft/yr ≈ 10⁻⁶ cm/sec and 1 cm/sec ≈ 2835 ft/day.
(c) All shear strengths, void ratios and permeabilities were determined on samples prepared at Standard Proctor maximum dry density and optimum moisture content.
(d) The values of cohesion, c_0 and c_{sat}, and friction angle, ϕ, are based on a straight-line Mohr strength envelope on effective stress axes as shown in Figure 3.7a (USBR, 1960). The value of c_{sat}, for the compacted-saturated condition was obtained by assuming that the frictional component of shear strength is not affected by saturation. Therefore, the friction angle, ϕ, also applies to the compacted-saturated condition. Consolidated-undrained (CU) triaxial tests with pore water pressure measurements were used to determine all the shear strengths.
(e) Since all laboratory tests, except large-sized permeability tests, were performed on the minus No. 4 (4.75 mm) fraction of soil, data on average values for gravels are not available for most properties. However, an indication as to whether these average values will be greater than or less than the average values for the corresponding sand group are given in the table (note entries with > or < symbol).
(f) Void ratio was derived from the maximum dry density and specific gravity of the soil grains.
(g) In USCS, there are no upper boundaries of liquid limit of MH and CH soils. The maximum limits for MH and CH soils tested by USBR (1960) were 81% and 88%, respectively. Soils with higher liquid limits than these will have inferior engineering properties.
(h) **The data in this table must not be used for design purposes. Design parameters must be developed based on project-specific testing.**

3. Case Studies of Embankment Failures

Stauffer and Wright (1984) and Kayyal and Wright (1991) investigated and documented a number of shallow failures in embankments. Thirty-four of the documented case histories were constructed from high plasticity clays known as Paris and Beaumont Clays, whose shear strength was experimentally investigated by Kayyal and Wright (1991). In addition to the information available from Stauffer and Wright (1984) and Kayyal and Wright (1991), climate records were retrieved from weather stations near the failure sites. Overall, the information available from the 34 failure case histories was found adequate for validating the ability of the numerical modeling approach developed by Morsy et al. (2023a) to predict time to failure. Information about the case histories is summarized in Table 2. The index properties of Paris and Beaumont Clays are summarized in Table 3.

Table 2. Summary of the Case Histories of Embankment Failures Simulated in this Study
Data in the table were compiled from Stauffer and Wright (1984) and Kayyal
and Wright (1991).

No.	Location[2]	Height, H (m)	Side Slope, λ (H:1V)	Fill Type	Construction Year	Failure Year	Time to Failure, TTF (years)
1	Loop 286 at T&P railroad (Missouri Pacific), SE Quadrant	6.1	3.0	Paris Clay	1965	1984	19
2	Loop 286 at SH 271 Interchange, NW Quadrant	4.3	2.5		1969	1983	14
3	Loop 286 at Missouri Pacific Railroad Overpass, SW Quadrant (North Slide)	8.2	2.9		1965	1983	18
4	Loop 286 at Missouri Pacific Railroad Overpass, SW Quadrant (South Slide)	9.0	2.8		1965	1983	18
5	Loop 286 at Missouri Pacific Railroad Overpass, NW Quadrant	8.4	2.7		1965	1983	18
6	Loop 286 at FM 79 Pacific, SW Quadrant	7.3	2.3		1964	1983	19
7	SH 271 North, SE of the Missouri Pacific Railroad South Embankment	6.4	2.8		1965[1]	1983[1]	18
8	Loop 286 and Still House Railroad Overpass (North) East Abutment	5.8	2.3		1965[1]	1983[1]	18
9	Loop 286 and Still House Railroad Overpass (North) West Abutment	6.7	3.0		1965[1]	1983[1]	18
10	Loop 286 and SH 271, NW Quadrant	4.9	2.7		1965[1]	1983[1]	18
11	Loop 286 and SH 271 Overpass (North) East Railroad	4.3	3.2		1965[1]	1983[1]	18
12	SH 271 North, SE of the Missouri Pacific Railroad North Embankment	4.9	2.7		1965[1]	1984[1]	19
13	SH 271 South, NW of the Missouri Pacific Railroad North Embankment	5.8	2.3		1965[1]	1984[1]	19
14	SH 271 South, SW of the Missouri Pacific Railroad North Embankment	5.8	2.3		1965[1]	1984[1]	19
15	SH 271 East, West of the Missouri Pacific Railroad North Embankment	6.4	3.0		1965[1]	1984[1]	19
16	SH 271 North, NW of the Missouri Pacific Railroad North Embankment	4.9	2.7		1965[1]	1984[1]	19
17	IH 610 at Scott St, NE Quadrant	5.8	2.5	Beaumont Clay	1966	1983	17
18	SH 225 at SH 146, SW Quadrant	4.6	3.0		1952	1983	31
19	SH 225 at SH 146, NW Quadrant	5.4	3.1		1952	1983	31
20	SH 225 at SH 146, SE Quadrant	4.1	3.4		1952	1983	31
21	SH 225 at Southern Pacific Railroad Overpass, SE Quadrant (West Slide)	8.1	2.6		1963	1983	20
22	SH 225 at Southern Pacific Railroad Overpass, SE Quadrant (East Slide)	5.9	3.1		1963	1983	20
23	SH 225 at Southern Pacific Railroad Overpass, SW Quadrant	7.2	2.4		1963	1983	20
24	SH 225 at Southern Pacific Railroad Overpass, NW Quadrant	3.1	3.1		1963	1983	20
25	SH 225 at Scarborough Ln, SE Quadrant	5.8	2.1		1966	1983	17
26	IH 610 at SH 225, SE Quadrant	5.3	2.7		1964	1983	19
27	IH 610 at Richmond St, SW Quadrant	7.8	2.7		1965	1983	18
28	IH 10 at Crosby-Lynchburg Rd, NW Quadrant	7.7	2.6		1958	1983	25
29	IH 45 at SH 146, SE Quadrant	4.7	3.0		1969	1983	14
30	IH 45 at SH 146, South Side	4.5	3.1		1969	1983	14
31	IH 45 at FM 2351, NE Quadrant	5.2	2.5		1971	1983	12
32	IH 45 at College St, NE Quadrant	3.5	3.0		1959	1977	18
33	US 59 at FM 525, NE Quadrant	5.0	2.4		1959	1983	24
34	US 59 at Shepard St, SE Quadrant	4.1	3.1		1961	1983	22

Notes:

[1] Construction and failure years were assumed based on the other reported cases in the investigation and the reported age at failure.

[2] IH stands for Interstate Highway; SH stands for State Highway; FM stands for Farm-to-Market Road; and US stands for US Highway.

Table 3. Index Properties and Classification of Clays Used in the Construction of the Embankment Case Histories (after Stauffer and Wright, 1984; Kayyal and Wright, 1991).

Parameter	Paris Clay	Beaumont Clay
Sand Fraction (0.075 mm < D ≤ 4.76 mm)	6%	11%
Silt Fraction (0.002 mm < D ≤ 0.075 mm)	36%	42%
Clay Fraction (D ≤ 0.002 mm)	58%	47%
Liquid Limit, LL	80	73
Plastic Limit, PL	22	21
Plasticity Index, PI	58	52
Activity, A	1.0	1.1
USCS	CH	CH
Specific Gravity, G_s	2.72	2.70
Bulk Unit Weight, γ_b (kN/m^3)	17.9	19.2
Optimum Moisture Content, ω_{opt} (%)	27.0	23.0
Void Ratio, e	0.73	0.62

4. Computer Models

FLAC (Fast Lagrangian Analysis of Continua) software v8.1 was used to create numerical models for the embankment failure case histories and conduct multi-phase, hydromechanical numerical simulations. The code used an explicit finite difference method to perform numerical computations of grided models for geotechnical engineering applications (Itasca 2019). The software allowed the performance of coupled multi-phase hydromechanical analyses. This study utilized the user-defined subroutines that were developed and implemented by Morsy et al. (2023a) to allow transient calculations of coupled hydromechanical behavior.

4.1 Model Description

The size of the mesh zones was selected to be equivalent to twice the typical thickness of embankment lift layers (2×0.25 m) to facilitate the simulation of the construction sequence, as shown in Figure 1. To minimize mesh zone size effects on the numerical results, the same mesh size was used for modeling embankment sections that were constructed with larger lift thicknesses. A non-local regularization approach was adopted in this study, which further minimizes the mesh size effects. To model the staged construction of embankment fill, the mesh layout was selected to accommodate horizontal layers of mesh zones. A detailed description of the model mesh and its development is provided in Morsy et al. (2023a). The geometries of the case histories modeled in this study were adapted to conform to the mesh layout using quadrilateral mesh zones 0.5 × 0.5 m. Subroutines were developed automatically to create the models that have various geometries with slope heights that are multiples of 0.5 m. Accordingly, the dimensions of the modeled embankments were approximated to the nearest 0.5 m.

The bottom boundary was constrained in both the horizontal and vertical directions. The lateral boundaries were constrained from displacement in the horizontal direction and were free to displace in the vertical direction. The thickness of the foundation layer in the model was selected to be twice the slope height from the embankment base, and its lateral extent was selected to be four times the slope height, as shown in Figure 1. The initial groundwater elevation was specified at a relatively large depth below the original ground surface (i.e., the base of the embankment) for all models. This assumption can be justified by the groundwater depths observed and documented in the Texas Water Development Board (TWDB) Groundwater Database (GWDB) for shallow groundwater observation wells in Lamar and Harris Counties for the period between 1952 through 1984, which is the service life range of the modeled case histories.

Prior to embankment construction, Effective vertical stresses were initialized at each mesh zone in the foundation soil using the effective overburden stress calculated at the respective depth. The effective lateral stresses were initialized by factoring the effective vertical stresses by an at-rest

coefficient, K_o, of 1.0.[2] To simulate embankment construction in this study, embankment layers were activated in the model incrementally, where each layer was loaded by a surcharge equivalent to the weight of the subsequent layer in a similar approach to the surface-pressure procedure (Lefebvre and Duncan, 1971; Palmerton and Lefebvre, 1972). A detailed description of model initialization and construction simulation is provided in Morsy et al. (2023a).

Figure 1. Finite-Difference Mesh Used to Model One Half of a Symmetrical Embankment

4.2 Climate Modeling

A transient climate boundary was defined at the surface of the model to simulate soil-atmosphere interaction. The climate boundary calculates the daily surface net flux as the difference between precipitation and actual evapotranspiration. Climate data collected from weather stations in the vicinity of the case histories were used to estimate reference evapotranspiration, ET_0, using the Penman-Monteith method, as adopted by FAO56 (Allen et al., 1998) for reference grass.[3] A daily average crop coefficient, K_c, was factored in the ET_o to account for Bermuda grasses, typically

---

[2] The at-rest coefficient of lateral earth pressure is the ratio of the horizontal effective stress to the vertical effective stress in soil at zero lateral strain condition.

[3] The Penman-Monteith method is a widely used formula for estimating evapotranspiration from a reference surface, incorporating climate parameters such as net radiation, air temperature, humidity, and wind speed.

grown in Texas, and its typical seasonal variation, as shown in Figure 2. The K_c values and periods of crop growth were selected based on FAO56 (Allen et al. 1998) for crops corresponding to those planted on the case study embankments. Figure 3 shows the weather data (1952 through 1984) developed for the annual cumulative precipitation and annual cumulative actual evapotranspiration. Note that the climate boundary was not activated in the numerical model until the end of embankment construction. A detailed description of the model climate boundary is provided in Morsy et al. (2023a).

Figure 2. Daily Average Crop Coefficient, K_c, for Typical Grass in a Typical Year at the Case Study Site Location
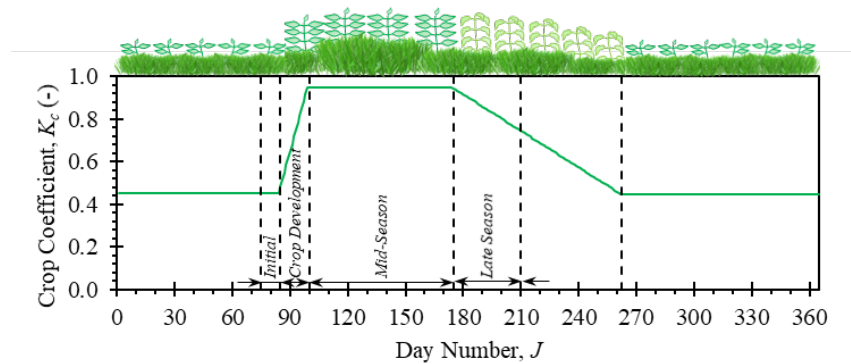
Figure 3. Climate Parameters Processed from Weather Data Obtained from
Weather Stations Near the Embankment Failure Case Histories
(a) annual cumulative evapotranspiration and
(b) annual cumulative precipitation
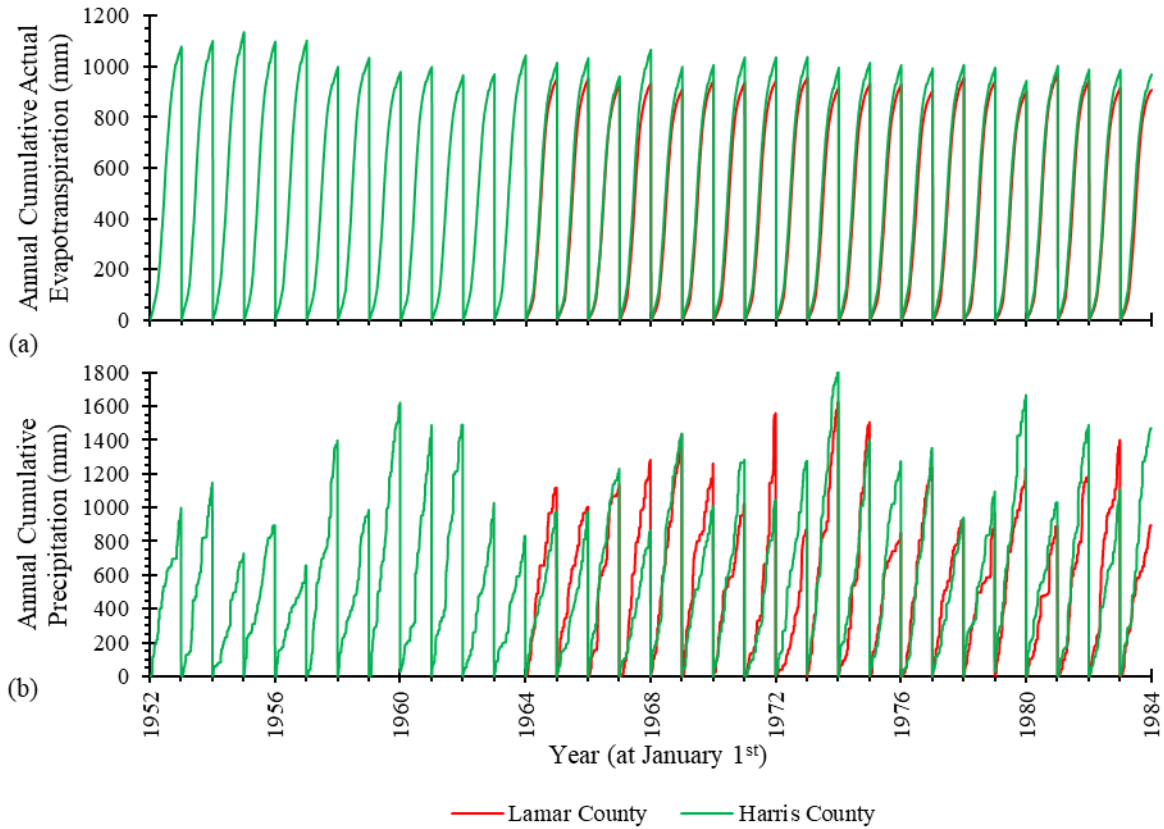

4.3 Mechanical Behavior Modeling

The mechanical behavior of the fill materials was modeled using a multi-stage Mohr-Coulomb model with strain softening (Potts and Zdrakovic, 1999) modified to simulate the change in mechanical behavior of clays with time (Morsy et al. 2023a).[4] In this model, the Mohr-Coulomb parameters, cohesion intercept, c, and angle of internal resistance, ϕ, and angle of dilation, ψ, vary with accumulated deviatoric plastic strain, ε_p, as shown in Figure 4a. Strength degradation incorporated in the embankment model includes two processes. The first process involves seasonal ratcheting plastic strain accumulation, which can be captured by the strain softening feature introduced to the constitutive model. The second process involves peak strength reduction due to wet-dry cycles in the near-surface, which was accounted for by reducing the peak strength

---

[4] The Mohr-Coulomb model is a mathematical model that describes the failure criteria of materials based on the relationship between shear strength and normal stress on a given shear plane.

parameters exponentially with time to their respective fully-softened strength parameters. This reduction can be approximated to the critical state strength parameters as shown in Figure 4b.

Figure 4. Conceptual Representation for the Shear Strength Constitutive Model Used to Idealize the Long-Term Behavior of Embankment Fill Prone to Strength Softening by Accumulated Plastic Strain and by Wet-Dry Cycles
(a) representation for a constitutive model. The shaded area represents the loss in peak strength of near-surface soil due to wet-dry cycles; and (b) representation for peak strength exponential decay of near-surface soil with number of seasonal wet-dry cycles (after Morsy et al., 2023a).

(a)   (b)
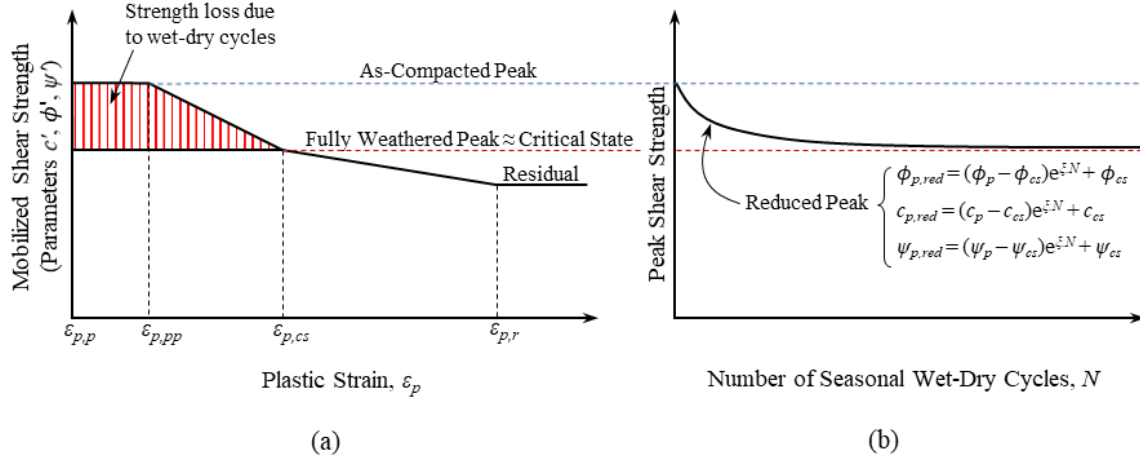
Young's modulus, E, of the soil was defined as a function in mean effective stress, σ'_m, as follows (suggested by Kulhawy et al., 1969).[5]

$$E = E_o p_o \left(\frac{\sigma'_m}{p_o}\right)^{m_E}, \quad \frac{\sigma'_m}{p_o} \geq 0.1 \qquad (1)$$

E_o is Young's modulus at 1 atm, p_o is the atmospheric pressure (1 atm), and m_E is the Young's modulus stress exponent. Poisson's ratio, υ, of the soil was defined as a function in mean effective stress, σ_m', as follows (suggested by Kulhawy et al., 1969).[6]

$$\upsilon = \upsilon_o - \ln\left(\frac{\sigma'_m}{p_o}\right)^{m_\upsilon}, \quad \frac{\sigma'_m}{p_o} \geq 0.1 \qquad (2)$$

υ_o is Poisson's ratio at 1 atm, p_o is the atmospheric pressure, and m_υ is the Poisson's ratio stress exponent. Mean effective normal stresses, σ'_m, were modeled based on Bishop's generalized effective stress (Bishop 1959) as $\sigma'_m = \sigma_m - u_a + \chi(u_a - u_w)$, where σ_m is the mean total normal

---

[5] Young's modulus is a measure of the stiffness of a material. It is defined as the ratio of stress to strain in the linear elastic region of the stress-strain curve.
[6] Poisson's ratio is a measure of the deformation of a material in directions perpendicular to the direction of loading. It is defined as the ratio of the lateral strain to the axial strain in a material subjected to uniaxial stress.

stress, u_a is the pore-air pressure, u_w is the pore-water pressure, and χ is Bishop's effective stress parameter and can be approximated to the degree of water saturation, S_w, for applications involving elevated degrees of water saturation, such as those in the current study (Khalili et al. 2004; Nuth and Laloui, 2008; Postill et al., 2021).

To calibrate the constitutive models for both the embankment fill and the foundation soil, isotropically-consolidated, undrained (CU) triaxial compression tests with pore-water pressure measurements were simulated using the numerical model (Kayyal and Wright, 1991). Table 4 summarizes the parameters of the shear strength and stiffness models used for both Paris Clay and Beaumont Clay. Figure 5 shows the numerical predictions obtained from the calibrated triaxial numerical model against the experimental data for both Paris and Beaumont Clays.

Table 4. Parameters of Shear Strength and Stiffness Models for Paris Clay and Beaumont Clay

Parameter		Paris Clay	Beaumont Clay
Peak friction angle	ϕ'_p (°)	20	24
Peak dilatancy angle	ψ'_p (°)	0	0
Peak cohesion intercept	c'_p (kPa)	8	20
Critical state friction angle	ϕ'_{cs} (°)	15	17
Critical state dilatancy angle	ψ'_{cs} (°)	0	0
Critical state cohesion intercept	c'_{cs} (kPa)	0	0
Residual friction angle	ϕ'_r (°)	10	12
Residual dilatancy angle	ψ'_r (°)	0	0
Residual cohesion intercept	c'_r (kPa)	0	0
Young's modulus at reference stress 1 atm	E_o (kPa)	400	230
Young's modulus stress exponent	m_E	0.35	0.25
Poisson's ratio at reference stress 1 atm	υ_o	0.3	0.3
Poisson's ratio stress exponent	m_υ	0.02	0.01

Figure 5. Comparison Between Experimental Measurements and Numerical
Predictions of Isotopically Consolidated Undrained Compression
Triaxial Tests for Paris and Beaumont Clays at Various Confining Stresses
(a) deviator stress versus axial strain for Paris Clay specimens, (b) change in pore pressure versus
axial strain for Paris Clay specimens, (c) deviator stress versus axial strain for Beaumont Clay
specimens, and (d) change in pore pressure versus axial strain for Beaumont Clay specimens.
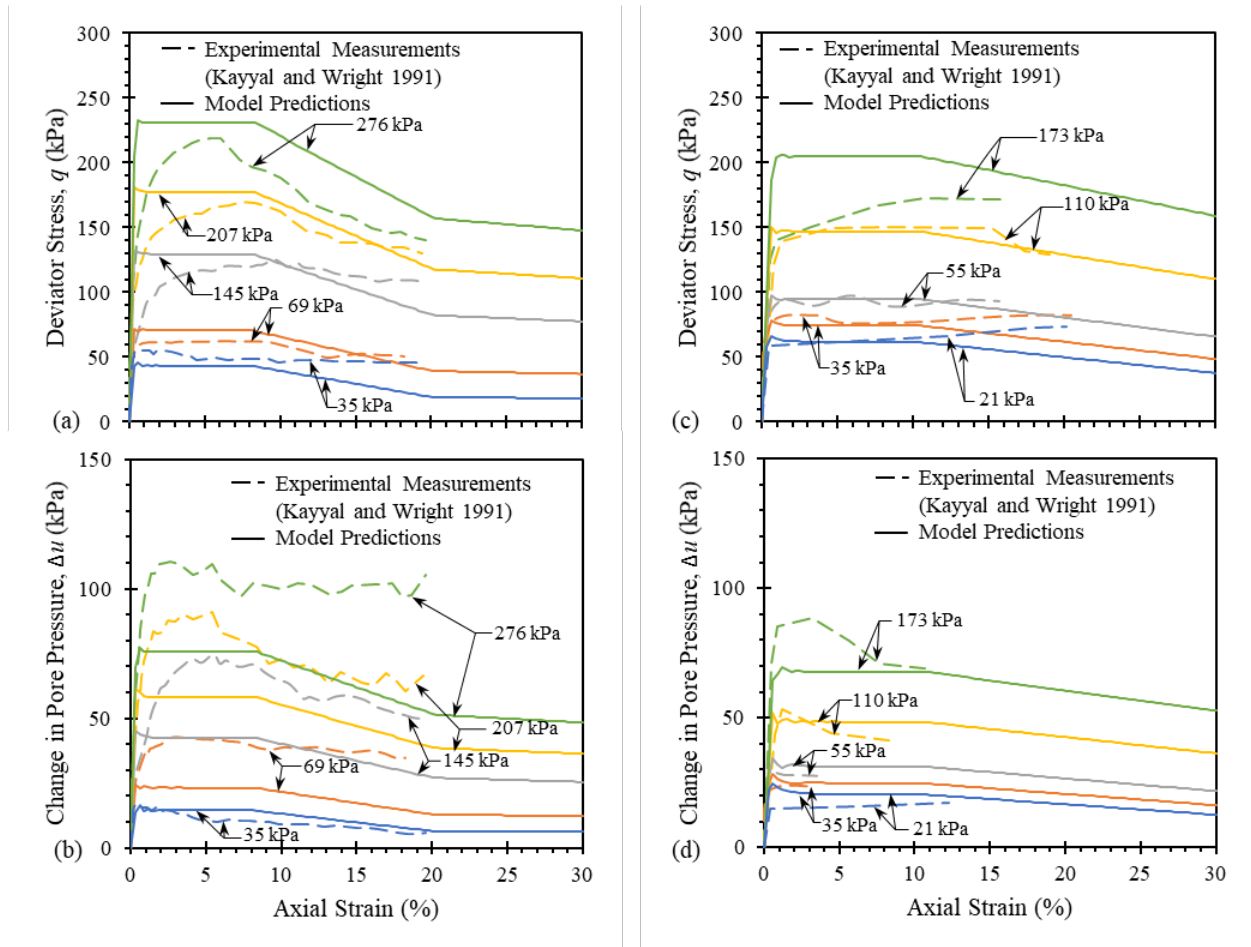
4.4 Hydraulic Behavior Modeling

Fluid transport in the finite-difference code used in this study is described by Darcy's law (Itasca, 2019).[7] The soil-water retention curves were developed based on van Genuchten (1980) fitting model for both the embankment fill and the foundation soil, as follows:

---

[7] Darcy's law is a law that describes the flow of fluid through a porous medium. The law states that the flow rate is proportional to the pressure difference and the permeability of the medium, and inversely proportional to the fluid's viscosity and the length of the flow path.

$$\psi_m = u_a - u_w = \psi_{m,o}\left(S_e^{-1/a_{vg}} - 1\right)^{1-a_{vg}} \qquad (3)$$

where ψ_m is the matric suction (i.e., the difference between the pore-air and pore-water pressures), $\psi_{m,o}$ a fitting parameter that can be related to the matric suction at air entry, a_{vg} is a fitting parameter, and S_e is the effective saturation, which can be expressed as $S_e = \frac{S_w - S_{w,r}}{1-S_{w,r}}$, where $S_{w,r}$ is the residual degree of water saturation. Since the pore fluids are treated as two immiscible fluids that can only displace each other within the void volume, the degree of gas saturation, S_g, can be expressed in terms of the degree of water saturation as $S_g = 1 - S_w$. The hydraulic conductivity functions were correlated to the soil-water retention curves using the van Genuchten-Mualem model (Mualem, 1976; van Genuchten, 1980) as $k_w = \kappa_{r,w}\ k_{w,sat}$, where k_w is the hydraulic conductivity, $k_{w,sat}$ is k_w at $S_w = 1$, and $\kappa_{r,w}$ is the relative expressed as follows:

$$\kappa_{r,w} = S_e^{b_{vg}}\left[1 - \left(1 - S_e^{1/a_{vg}}\right)^{a_{vg}}\right]^2 \qquad (4)$$

where b_{vg} is a fitting parameter. The air conductivity functions were correlated to those of the hydraulic conductivity (Itasca 2019) as $k_g = \kappa_{r,g}\ k_{g,sat}$, where k_g is the gas conductivity, and $k_{g,sat}$ is k_g at $S_w = 1$, which was correlated to the saturated hydraulic conductivity and water-to-air dynamic viscosity ratio, μ_r, as $k_{g,sat} = \gamma_g\ \mu_r\ k_{w,sat}$, and $\kappa_{r,g}$ is the relative gas conductivity, which can be expressed as follows:

$$\kappa_{r,g} = (1 - S_e)^{c_{vg}}\left(1 - S_e^{1/a_{vg}}\right)^{2a_{vg}} \qquad (5)$$

where c_{vg} is a fitting parameter. In the absence of data necessary to develop the hydraulic models of Paris and Beaumont Clays, the parameters of the hydraulic models were estimated based on the experimental data for Paris and Houston Clays reported by Puppala et al. (2013). It should be noted that the soils tests by Puppala et al. (2013) are not necessarily identical to those tested by Kayyal and Wright (1991). However, they were obtained from the same areas as those of Paris and Beaumont Clays and are believed to have undergone similar geological processes. The soil water retention model parameters derived for Paris and Beaumont Clays are summarized in Table 5. Figure 6a presents the soil-water and soil-gas retentivity functions, and Figure 6b presents the hydraulic and gas conductivity functions.

The saturated hydraulic conductivity, $k_{w,sat}$, was correlated to the void ratio, e, according to the empirical formula proposed by Samarasinghe et al. (1982) as $k_{w,sat} = C\left(\frac{e^l}{1+e}\right)$, where C and l are empirical parameters, which were selected based on correlations between $k_{w,sat}$ and e for clays (Babaoglu and Simms, 2020) for both Paris and Beaumont Clays and are summarized in Table 5. The C parameter was taken as 1×10^{-7} m/s for near-surface weathered soil. A constant value of $k_{w,sat} = 1\times10^{-12}$ m/s was used for the foundation soil.

Table 5. Hydraulic Parameters for Soil-Fluid Retentivity and Fluid Conductivity Functions for Paris and Beaumont Clays

Parameter		Value
Compacted Saturated Hydraulic Conductivity Parameter	C (m/s)	1×10^{-8}
Compacted Saturated Hydraulic Conductivity Parameter	l	5.00
Soil-Water Retention Model Fitting Parameter	a_{vg}	0.23
Hydraulic Conductivity Function Fitting Parameter	b_{vg}	0.50
Gas Conductivity Function Fitting Parameter	c_{vg}	0.50
Soil-Water Retention Model Fitting Parameter	$\psi_{m,o}$ (kPa)	300
Residual Degree of Water Saturation	$S_{w,r}$	0.00
Water-To-Air Dynamic Viscosity Ratio	μ_r	55

Figure 6. Fluid Models for Paris and Beaumont Clays
(a) soil-water and soil-gas retentivity functions;
and (b) hydraulic and gas conductivity functions.

(a)

(b)
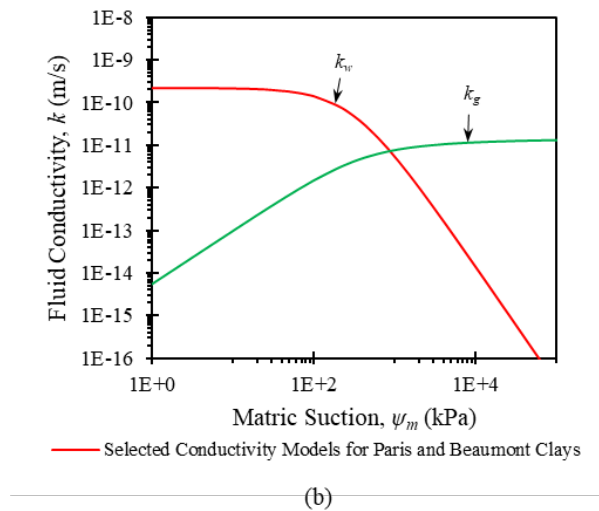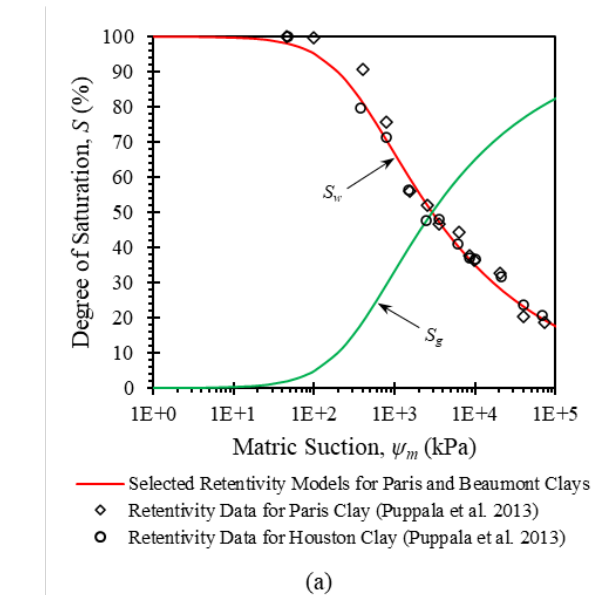
5. Failure Prediction

The ultimate goal of this study is to develop a numerical tool capable of predicting the time of failure occurrence. Factor of safety was used as a performance indicator to evaluate time to failure. Factor of safety is a widely used metric in slope stability assessment in practice. The failures involved in this study are shallow, typically involving a surficial sliding soil block along a slip surface that is practically parallel to the slope surface. The factor of safety of a slope in this condition can be determined using a simplified, infinite-slope stability analysis procedure, considering unsaturated soil conditions. The factor of safety for a slip surface at a depth z from the slope surface, FoS, can be expressed as $FoS = \frac{\tau_f}{\tau}$, where τ_f is the shear strength at depth z; τ_f can be expressed as follows:

$$\tau_f = c' + [\sigma_v \cos^2 \alpha - (1 - S_w)u_a - S_w u_w]\tan \phi' \qquad (6)$$

where σ_v is the vertical normal stress at depth z, τ is the shear stress at depth z, and can be written as follows:

$$\tau = \sigma_v \cos \alpha \sin \alpha \qquad (7)$$

Figure 7. Typical Factor of Safety, FoS, Profiles with Depth at the Time of Predicted Failure for Two Example Models
(a) Case 25 involving Beaumont Clay and (b) Case 1 involving Paris Clay

(a)   (b)
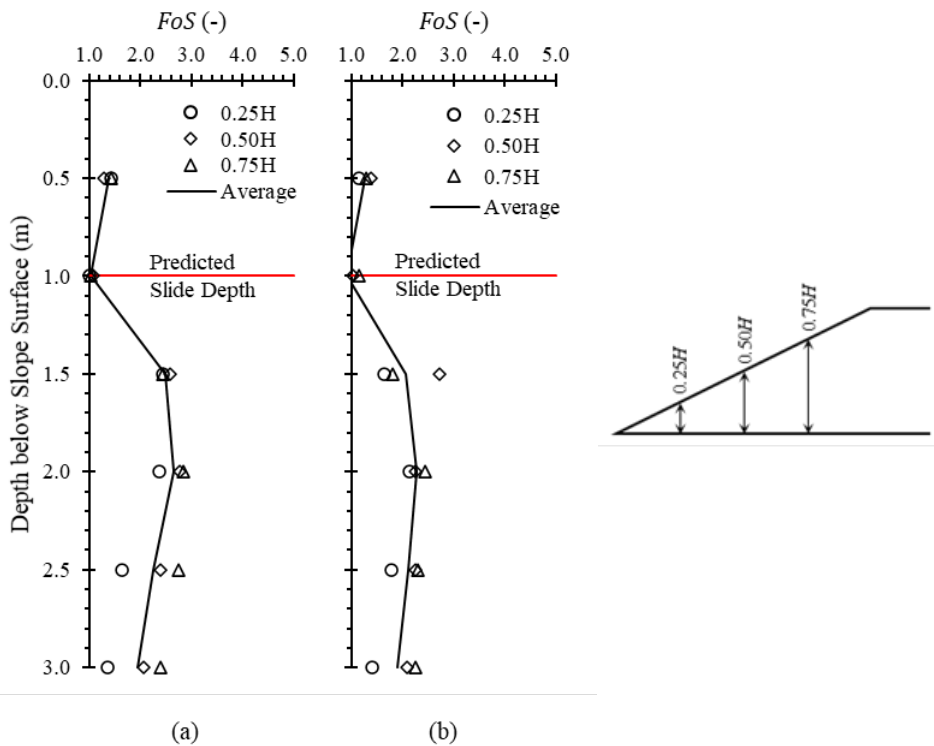
The minimum FoS was determined as the lowest FoS within the topmost 3 m of the slope at any given time during the slope service age. The search was limited to 3 m since this is the zone where weather-driven shallow slides are expected to occur. It was also the zone within which slides appeared for the modeled case histories, as reported by Kayyal and Wright (1991). Figure 7 shows typical FoS profiles with depth at the time of predicted failure for Cases 25 and 33. The profiles were plotted at different locations along the slope: 1/4, 2/4, and 3/4 of slope height, H. Minimum FoS was predicted for both cases at a depth 1 m from the slope surface. It was evident for most cases that the FoS values along the slope converged at the slide depth, which supports the assumption that the FoS calculated for the modeled slopes can be approximated to that of infinite slopes.

The minimum FoS, variation with time during the service life predicted by numerical models for Cases 1 through 16 (embankments constructed with Paris Clay) are shown in Figures 8a through Figure 8p, respectively. These values of FoS were calculated based on numerical model predictions of shear strength and stress. As expected, it was observed that FoS during wet seasons is the lowest, with further reduction every subsequent wet season approaching 1.0. The actual time to failure, TTF_{actual}, reported by Kayyal and Wright (1991) for each case is annotated on the respective subfigure for comparison.

The minimum FoS, variation with time during the service life predicted by numerical models for Cases 17 through 34 (embankments constructed with Beaumont Clay) are shown in Figures 9a through Figure 9r, respectively. The actual time to failure, TTF_{actual}, reported by Kayyal and Wright (1991) for each case is annotated on the respective subfigure for comparison. The models of these cases did not show a sudden slope collapse. Instead, progressive, increased deformation occurred with service time, accompanied by progressive reduction in shear strength and FoS to values equal or close to 1.0. This is attributed to the small strain softening rate of Beaumont Clay which retains adequate soil shear strength with increasing plastic strain. It is believed that improved shear strength testing of Beaumont Clay could improve the constitutive model of this soil, especially at large shear strains. However, with the existing knowledge, failure of slopes constructed with Beaumont Clay could be predicted by computing the FoS with time, using numerical predictions of shear strength and stress. Time to failure in this condition could be defined as the time to FoS = 1.0 (i.e., theoretical infinite slope failure) or other conservative criteria that infrastructure stakeholders may adopt (e.g., time to FoS = 1.1, 10 years prior to FoS = 1.0).

Figure 8. Minimum Annual Factor of Safety, FoS, Variation with Service Age

Subfigures (a) through (p) show the predicted minimum annual FoS for Cases 1 through 16, respectively. Approximate actual time to failure, TTF_{actual}, reported by Kayyal and Wright (1991) is marked for each case on its respective subfigure.
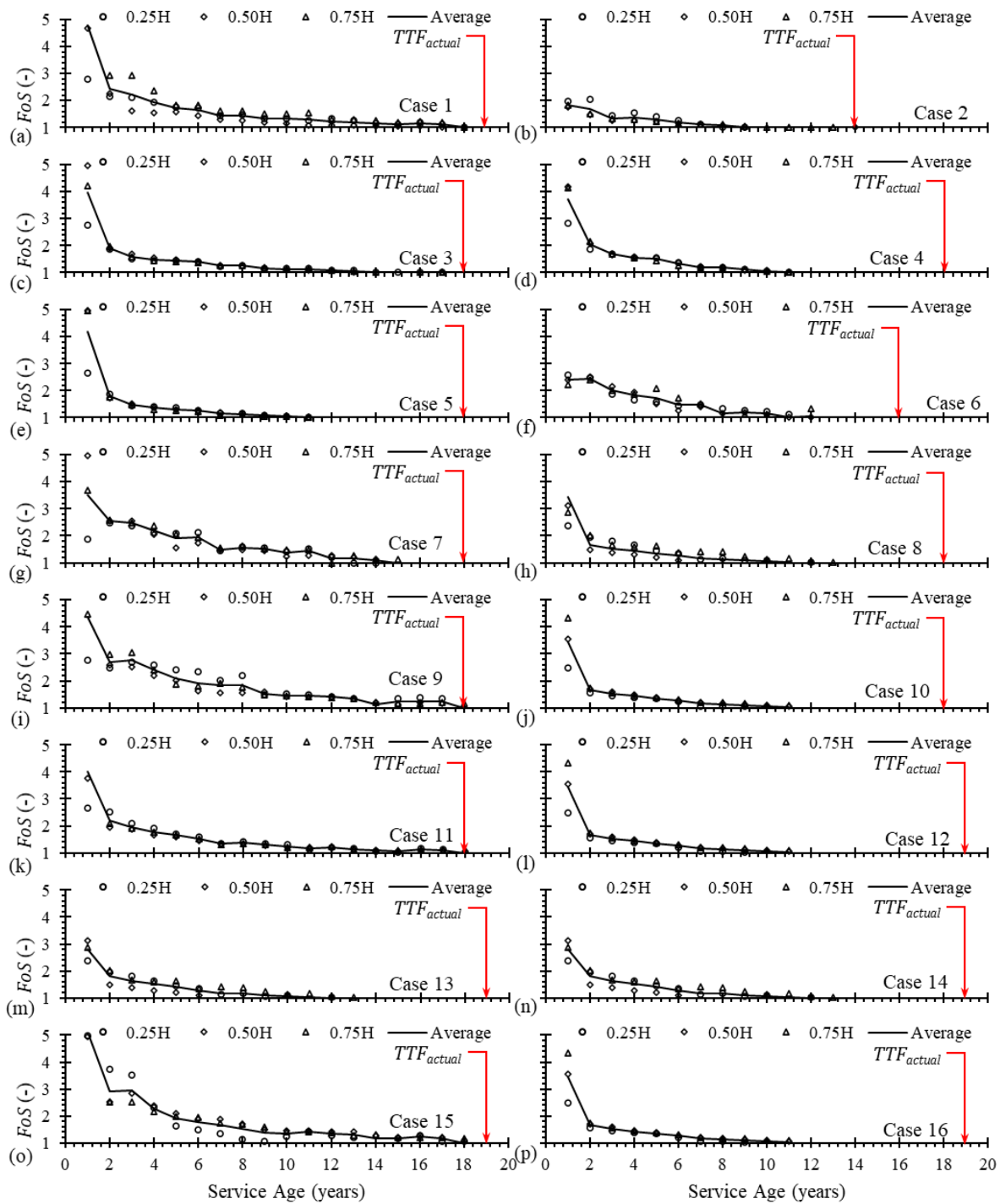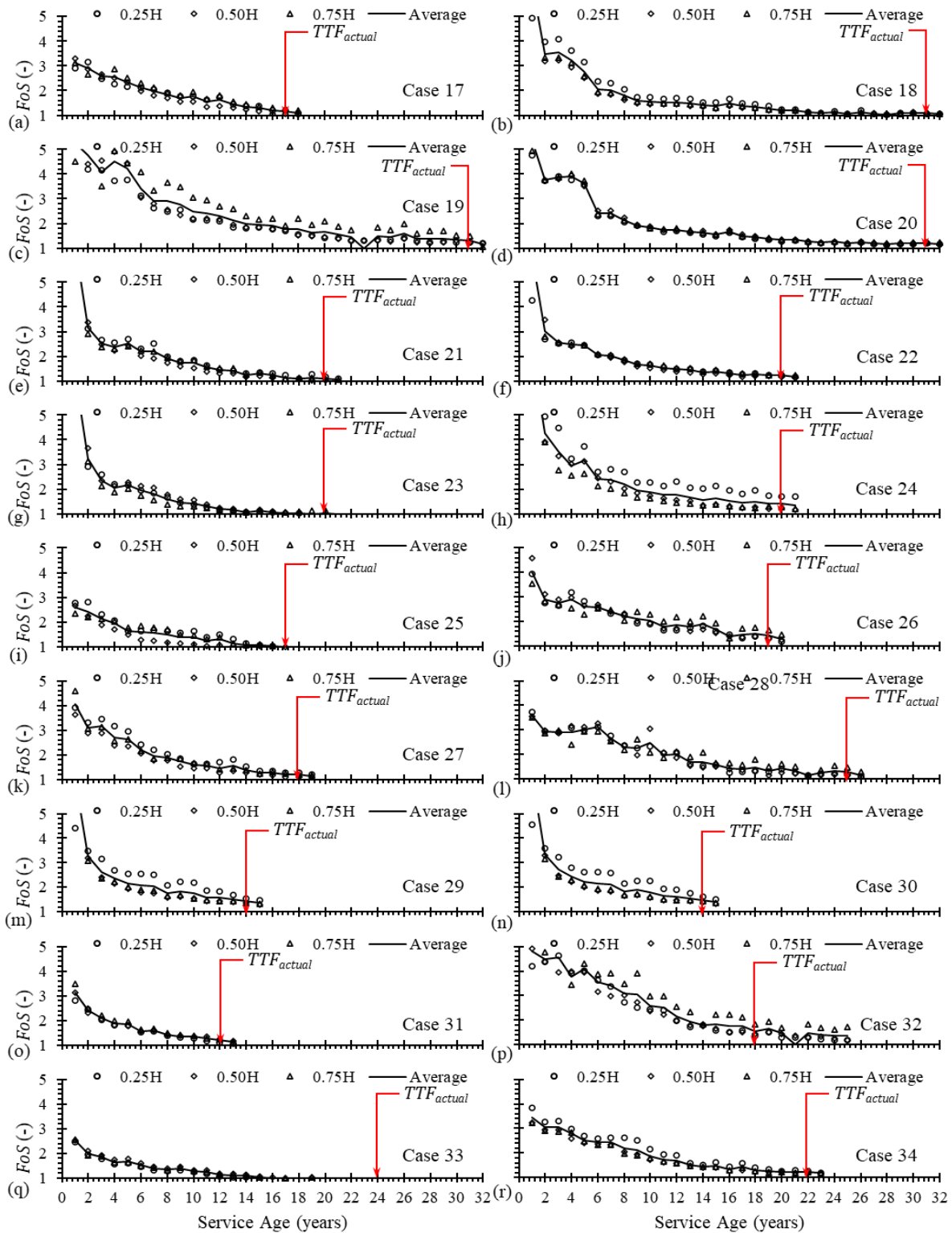
Figure 9. Minimum Annual Factor of Safety, FoS, Variation with Service Age
Subfigures (a) through (r) show the predicted minimum annual FoS for Cases 17 through 34,
respectively. Approximate actual time to failure, TTF_actual, reported by Kayyal and Wright (1991)
is marked for each case on its respective subfigure.

Table 6 summarizes the predicted time to the minimum FoS for each simulated case history. A comparison between predicted time to minimum FoS and actual time to failure reported by Kayyal and Wright (1991) is presented in Figure 10. Twenty-two case history models reached a minimum FoS = 1.0 by the actual TTF; six case history models reached a minimum FoS = 1.1 by the actual TTF; four case history models reached a minimum FoS = 1.2 by the actual TTF; and two case history models reached a minimum FoS = 1.3 by the actual TTF. Note that for the two cases whose FoS dropped to only 1.3 by the actual TTF, their actual TTF is 14 years, which is much less than other comparable cases with similar geometries. Being subject to variability, the actual TTF for the various cases modeled in this study did not follow strong trends regarding slope properties. Overall, the majority of the numerical models developed in this study were able, to a large level of accuracy, to predict the time to failure of weather-driven shallow slides in clay embankments.

Table 6. Summary of the Predicted Minimum Factors of Safety, FoS,
and their Corresponding Service Life
Actual times to failure reported by Kayyal and Wright (1991) are included for comparison.

Case History Number	Predicted Minimum FoS (-)	Predicted Time to FoS = 1.0 (years)	Predicted Time to FoS = 1.1 (years)	Predicted Time to FoS = 1.2 (years)	Actual Time to Failure (years)
Case 1	1.0	18	-	-	19
Case 2	1.0	13	-	-	14
Case 3	1.0	17	-	-	18
Case 4	1.0	10	-	-	18
Case 5	1.0	10	-	-	18
Case 6	1.0	11	-	-	19
Case 7	1.0	14	-	-	18
Case 8	1.0	13	-	-	18
Case 9	1.0	17	-	-	18
Case 10	1.0	10	-	-	18
Case 11	1.0	17	-	-	18
Case 12	1.0	10	-	-	19
Case 13	1.0	13	-	-	19
Case 14	1.0	13	-	-	19
Case 15	1.0	17	-	-	19
Case 16	1.0	10	-	-	19
Case 17	1.0	18	-	-	17
Case 18	1.0	27	-	-	31
Case 19	1.2	-	-	27	31
Case 20	1.1	-	32	-	31
Case 21	1.0	20	-	-	20
Case 22	1.1	-	21	-	20
Case 23	1.0	19	-	-	20
Case 24	1.1	-	20	-	20
Case 25	1.0	17	-	-	17
Case 26	1.2	-	-	19	19
Case 27	1.1	-	19	-	18
Case 28	1.1	-	26	-	25
Case 29	1.3	-	-	-	14
Case 30	1.3	-	-	-	14
Case 31	1.2	-	-	13	12
Case 32	1.2	-	-	24	18
Case 33	1.0	18	-	-	24
Case 34	1.1	-	23	-	22

Figure 10. Comparison Between Predicted Time to Minimum Factor of Safety, FoS,
and Actual Time to Failure Reported by Kayyal and Wright (1991)
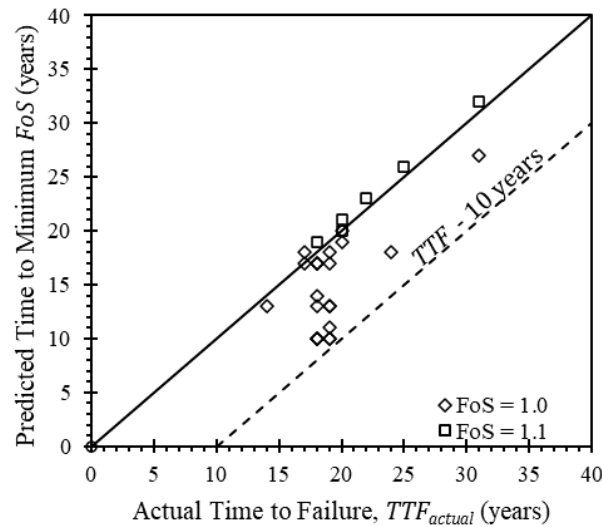
This study shows that shallow slides in clay embankments are likely to happen when the near-surface soil is almost saturated, and pore pressure is nearly zero. The study also shows that the cohesion intercept shear-strength parameter is likely to drop near zero at the time of failure. The theoretical factor of safety calculation for infinite slopes was found to predict failure well, as evidenced by the numerical results of Cases 1 through 16. Accordingly, this study suggests that the slope angle, α, be equal to critical state friction angle, ϕ_{cs}, of the embankment fill. Achieving an FoS of 1.1 to 1.2 may be reasonable, considering that pore pressure drops to zero during a temporary period. Therefore, an acceptable slope angle can be expressed as follows:

$$\alpha = \tan^{-1}\left(\frac{\tan \phi_{cs}}{FoS}\right) \qquad (8)$$

Preventive measures that may reduce the risk of swelling-induced shallow failures include (1) vegetation that can provide reinforcement to the near-surface soil through their roots and promote evapotranspiration to reduce swelling potential and (2) mixing cementing agents, such as lime, into the near-surface soil to reduce swelling potential.

6. Summary and Recommendations

This study aimed to predict the time to failure of aging, deteriorating clay embankments supporting transportation infrastructure. A multi-phase numerical modeling approach was developed to simulate the long-term, weather-driven hydromechanical behavior of clay embankments. This approach was used to develop models for a total of 34 failure case studies with known time to failure. A comparison was made between predicted time to minimum FoS and actual time to failure. Overall, the majority of the numerical models developed in this study were able, to a large level of accuracy, to predict the time to failure of weather-driven shallow slides in clay embankments. The study recommends that FoS is calculated considering infinite slope failure at depths up to 3 m below the slope surface, and considering zero pore pressure, a critical state friction angle, ϕ_{cs}, and a zero-cohesion intercept. Considering the typical recommended minimum FoS values by Caltrans, an FoS of 1.1 to 1.2 may be reasonable for existing embankments, given the temporary nature of the conditions causing shallow slides. For new designs, an FoS of 1.3 may be recommended.

Bibliography

Allen, R.G., Pereira, L.S., Raes, D., and Smith, M. (1998). Crop evapotranspiration-Guidelines for computing crop water requirements-FAO Irrigation and drainage paper 56. FAO, Rome, 300(9), D05109.

Babaoglu, Y., and Simms, P. (2020). "Improving hydraulic conductivity estimation for soft clayey soils, sediments, or tailings using predictors measured at high-void ratio." *Journal of geotechnical and geoenvironmental engineering*, Vol. 146, No. 10, 06020016.

Baral, A., and Shahandashti, S. M. (2022). "Identifying critical combination of roadside slopes susceptible to rainfall-induced failures." *Natural Hazards*, DOI: 10.1007/s11069-022-05343-6.

Beckstrand, D., and Bunn, M. (2024). *Prevention and Mitigation of Surficial Slope Failures on Fill Highway Embankment Slopes*. NCHRP Synthesis 617, National Academies of Sciences, Engineering, and Medicine (NASEM), Washington, DC: The National Academies Press. https://doi.org/10.17226/27645.

Bishop, A.W. (1959). "The principle of effective stress." *Teknisk ukeblad*, Vol. 39, pp. 859-863.

Briggs, K. M., Helm, P. R., Smethurst, J. A., Smith, A., Stirling, R., Svalova, A., ... & Glendinning, S. (2023). "Evidence for the weather-driven deterioration of ageing transportation earthworks in the UK." *Transportation Geotechnics*, 101130. DOI: 10.1016/j.trgeo.2023.101130

Caltrans Geotechnical Manual (2024). *Caltrans Geotechnical Manual*, California Department of Transportation.

Caltrans Highway Design Manual (2020). *Highway Design Manual*. Seventh Edition, California Department of Transportation, Sacramento, CA.

Cheng, Q., Tang, C. S., Zeng, H., Zhu, C., An, N., and Shi, B. (2020). "Effects of microstructure on desiccation cracking of a compacted soil." *Engineering Geology*, Vol. 265, 105418.

FHWA (2006). *Soils and Foundations*. Volumes I and II, Report No. FHWA-NHI-06-088 and FHWA-NHI-06-089, Authors: Samtani, N.C. and Nowatzki, E.A., Federal Highway Administration, U.S. Department of Transportation, Washington, DC.

Itasca (2019). *Fast Lagrangian Analysis of Continua V. 8.1 – User's Guide*. 1st edition, Itasca Consulting Group Inc., Minneapolis, US.

Kayyal, M.K., and Wright, S.G. (1991). *Investigation of long-term strength properties of Paris and Beaumont clays in earth embankments.* Report No. FHWA/TX-92+1195-2F, Center for Transportation Research, the University of Texas at Austin, November 1991, Austin, Texas, US.

Khalili, N., Geiser, F., and Blight, G.E. (2004). "Effective Stress in Unsaturated Soils: Review with New Evidence." *International Journal of Geomechanics*, Vol. 4, pp. 115–126.

Kovacevic, N., Hight, D.W., Potts, D.M., and Carter, I.C. (2013). "Finite-element analysis of the failure and reconstruction of the main dam embankment at Abberton Reservoir, Essex, UK." *Geotechnique*, Vol. 63, pp. 753–767.

Kulhawy, F.H., Duncan, J.M., and Seed, H.B. (1969). *Finite element analyses of stresses and movements in embankments during construction.* U.S. Army Engineer Waterways Experiment Station, Vicksburg, Mississippi, US.

Lees, A.S., MacDonald, G.J., Sheerman-Chase, A., and Schmidt, F. (2013). "Seasonal slope movements in an old clay fill embankment dam." *Canadian Geotechnical Journal*, Vol. 50, No. 5, pp. 503-520.

Lefebvre, G., and Duncan, J.M. (1971). *Three-dimensional finite element analyses of dams.* Report No. TE 71-5, US Army Engineers Waterways Experiment Station, Corps of Engineers, Vicksburg, Mississippi, US.

Morsy, A.M., Helm, P.R., El-Hamalawi, A., Smith, A., Hughes, P.N., Stirling, R.A., Dijkstra, T.A., Dixon, N., and Glendinning, S. (2023a), "Development of a Multi-Phase Numerical Modeling Approach for Hydromechanical Behavior of Clay Embankments Subject to Weather-Driven Deterioration," *Journal of Geotechnical and Geoenvironmental Engineering*, Vol. 149, No. 8.

Morsy, A.M., Helm, P.R., El-Hamalawi, A., Smith, A., Hughes, P.N., Stirling, R.A., Dijkstra, T.A., Dixon, N., and Glendinning, S. (2023b). *Data Used for the Validation of the BIONICS Research Embankment Hydromechanical Model.* Dataset, Newcastle University. DOI: 10.25405/data.ncl.22144442

Morsy, A.M., Helm, P.R., El-Hamalawi, A., Smith, A., and Stirling, R.A. (2024), "Simulation of Weather-Driven Deterioration of Clay Embankments," In *Proceedings of Geo-Congress 2024*, American Society of Civil Engineers (ASCE), February 25-28, 2024 | Vancouver, BC, Canada, pp. 85-94. DOI: 10.1061/9780784485354.009

Mualem, Y. (1976). "A new model for predicting the hydraulic conductivity of unsaturated porous media." *Water Resources Research*, Vol. 12, No. 3, pp. 513-522.

NASEM (2019). *Geotechnical Asset Management for Transportation Agencies, Volume 1: Research Overview.* Report NCHRP 903, Washington, DC: The National Academies Press. https://doi.org/10.17226/25363

Nuth, M., and Laloui, L. (2008). "Effective stress concept in unsaturated soils: Clarification and validation of a unified framework." *International journal for numerical and analytical methods in Geomechanics*, Vol 32, no. 7, pp. 771-801.

Nyambayo, V. P., and Potts, D. M. (2010). "Numerical simulation of evapotranspiration using a root water uptake model." *Computers and Geotechnics*, Vol. 37, No. 1-2, pp. 175-186.

Nyambayo, V.P., Potts, D.M., and Addenbrooke, T.I. (2004). "The Influence of permeability on the stability of embankments experiencing seasonal cyclic pore water pressure changes." In *Proceedings of Advances in geotechnical engineering: The Skempton conference*, London, UK, March 2004, pp. 898-910.

Palmerton, J.B., and Lefebvre, G. (1972). *Three-dimensional finite element analyses of dams.* Report No. S 72-1, US Army Engineers Waterways Experiment Station, Corps of Engineers, Vicksburg, Mississippi, US.

Postill, H., Helm, P. R., Dixon, N., Glendinning, S., Smethurst, J. A., Rouainia, M., Briggs, K.M., El-Hamalawi, A., and Blake, A.P. (2021). "Forecasting the long-term deterioration of a cut slope in high-plasticity clay using a numerical model." *Engineering Geology*, Vol. 280, 105912.

Potts, D.M., and Zdravkovic, L. (1999). Finite element analysis in geotechnical engineering: theory. Thomas Telford, London, UK.

Puppala, A.J., Manosuthikij, T., and Chittoori, B.C. (2013). "Swell and shrinkage characterizations of unsaturated expansive clays from Texas." *Engineering Geology*, Vol. 164, pp. 187-194.

Rouainia, M., Davies, O., O'Brien, T., and Glendinning, S. (2009). "Numerical modelling of climate effects on slope stability." *Proceedings of the Institution of Civil Engineers-Engineering Sustainability*, Vol. 162, pp. 81-89.

Samarasinghe, A.M., Huang, Y.H., and Drnevich, V.P. (1982). "Permeability and consolidation of normally consolidated soils." *Journal of the Geotechnical Engineering Division*, Vol. 108, No. 6, pp. 835-850.

Samtani, N.C., and Nowatzki, E.A. (2021). *Mechanically Stabilized Earth (MSE) Wall Fills—A Framework for Use of Local Available Sustainable Resources (LASR).* Report No. FHWA-HIN-21-002. Federal Highway Administration (FHWA): Washington, DC, US.

Shahandashti, M., Hossain, S., Khankarli, G., Zahedzahedani, S.E., Abediniangerabi, B., and Nabaei, M. (2019). *Synthesis on rapid repair methods for embankment slope failure*. Report No. FHWA/TX-18/0-6957-1, Texas Department of Transportation.

Skempton, A.W. (1964). "Long-term stability of clay slopes." *Geotechnique*, Vol. 14, pp. 77-102.

Skempton, A.W. (1996). "Embankments and cuttings on the early railways." *Construction History*, Vol 11, pp. 33-49.

Stauffer, P. A., and Wright, S. G. (1984). *An examination of earth slope failures in Texas*. Report No. FHWA-TX-86-06+ 353-3F.

Stirling, R.A., Toll, D.G., Glendinning, S., Helm, P.R., Yildiz, A., Hughes, P.N., and Asquith, J.D. (2021). "Weather-driven deterioration processes affecting the performance of embankment slopes." *Géotechnique*, Vol. 71, No. 11, pp. 957-969.

Take, W.A., and Bolton, M.D. (2011). "Seasonal ratcheting and softening in clay slopes, leading to first-time failure." *Geotechnique*, Vol. 61, pp. 757-769.

Tang, D., Jiang, Z., Yuan, T., and Li, Y. (2020). « Stability analysis of soil slope subjected to perched water condition." *KSCE Journal of Civil Engineering*, Vol. 24, No. 9, pp. 2581-2590.

Templeton, A.E., Sills, G.L., and Cooley, L.A. (1984). "Long term failure in compacted clay slopes." In *Proceedings of International Conference on Case Histories in Geotechnical Engineering*, pp. 749-754.

USBR (1960). *Design of Small Dams*. 1st Edition. U.S. Department of the Interior, Bureau of Reclamation, Washington, DC.

van Genuchten, M.T. (1980). "A closed-form equation for predicting the hydraulic conductivity of unsaturated soils." *Soil Science Society of America Journal*, Vol. 44, No. 5, pp. 892-898.

Vaughan, P.R., Kovacevic, N., and Potts, D.M. (2004). "Then and now: some comments on the design and analysis of slopes and embankments." In *Proceedings of Advances in Geotechnical Engineering: The Skempton Conference*, pp. 241-290.

Walkinshaw, J. (1992). "Landslide correction costs on US state highway systems." *Transportation Research Record*, Vol. 1343, pp. 36-41.

About the Author

Amr M. Morsy, PhD, PE

Dr. Amr Morsy is a professional civil engineer with experience in both academia and industry with focus on geotechnical engineering, transportation geotechnics, environmental geotechnics, and climate adaptation. He obtained his B.Eng and M.Sc. degrees in civil engineering from Cairo University in 2011 and 2013, respectively, and obtained his PhD degree in civil engineering from The University of Texas at Austin in 2017. He worked as a postdoctoral fellow at The University of Texas at Austin in 2018 and as practicing geotechnical engineer from 2018 to 2020. He later worked as a research associate at Loughborough University on the ACHILLES program grant from 2020 to 2022. He has been working as an assistant professor at California State University Long Beach since 2022.

As part of his academic experience, Dr. Morsy conducts research on geotechnical infrastructure deterioration and asset management, climate change impacts on geotechnical infrastructure, and geotechnical solutions for a sustainable built environment. He has excelled in physical and numerical modeling of geotechnical and geoenvironmental engineering systems and in infrastructure instrumentation and laboratory experimentation. He participated in research projects sponsored by the Transportation Research Board of the National Academies of Sciences, Engineering, and Medicine, the Engineering and Physical Sciences Research Council of the UK Research and Innovation, the US Federal Highway Administration, the Geosynthetic Institute, Texas and Indiana Departments of Transportation, and geosynthetic manufacturers.

As part of his professional consulting experience, Dr. Morsy conducts rigorous analyses, designs, and forensic evaluations for a range of slopes, retaining walls, reinforced soil structures, deep excavations, bridge foundations, waste containment facilities, and tailings and embankment dams. He assisted expert witnesses in cases involving collapse and poor performance of earth retaining structures. He provided solutions to geotechnical problems in a number of environmental remediation projects involving cleanup of superfund sites. He conducted multi-phase flow analyses for several infrastructure features including earthworks, embankment dams, and cover systems. Some of the consulting projects he participated in served the US Environmental Protection Agency, New York State Department of Environmental Conservation, New York State and Indiana Departments of Transportation, Tennessee Valley Authority, New Jersey Transit, and several multinational private and public corporations.